Original Article

Mechanical Load Increases in Bone Formation Via a Sclerostin-Independent Pathway[†]

A Morse[1,2*], MM McDonald[3], NH Kelly[4,5], KM Melville[4,5], A Schindeler[1,2], I Kramer[6], M Kneissel[6], MCH van der Meulen[4,7], and DG Little[1,2]

1 Orthopaedic Research & Biotechnology Unit, The Children's Hospital at Westmead, Sydney, Australia
2 Discipline of Paediatrics and Child Health, Sydney Medical School, University of Sydney, Sydney, Australia
3 Bone Biology Program, The Garvan Institute of Medical Research, Sydney, Australia
4 Sibley School of Mechanical and Aerospace Engineering, Cornell University, Ithaca, United States
5 Biomedical Engineering, Cornell University, Ithaca, NY, USA
6 Novartis Pharma, Basel, Switzerland
7 Hospital for Special Surgery, New York, United States

*** Corresponding author and reprint address:**
Alyson Morse
Orthopaedic Research and Biotechnology
The Children's Hospital at Westmead
Locked Bag 4001,
Westmead, NSW, 2145, Australia
Email: alyson.morse@sydney.edu.au
Phone: +61-2-98451452
Fax: +61-2-98453078

Authors Major Degree:
Morse A, B.Biotech(Hons)
McDonald MM, PhD
Kelly NH, BME
Melville KM, M.S.
Schindeler A, PhD
Kramer I, PhD
Kneissel M, PhD
van der Meulen MCH, PhD
Little DG, FRACS(Orth), PhD

Keywords: Mechanotransduction, Loading, Bone, Unloading, Sclerostin, WNT

Abbreviations: BTX (botulinum toxin), LRP (low-density-lipoprotein receptor-related protein), RANKL (Receptor activator of nuclear factor kappa-B ligand), OPG (osteoprotegerin), Dkk1 (Dickkopf-1), DXA (dual-energy x-ray absorptiometry), CT (computed tomography), VOI (volume of interest), WT (wild type), ERα (estrogen receptor α), insulin-like growth factor I (IGF-I).

Additional Supporting Information may be found in the online version of this article.

Initial Date Submitted February 23, 2014; Date Revision Submitted April 22, 2014; Date Final Disposition Set May 6, 2014

Journal of Bone and Mineral Research

DOI 10.1002/jbmr.2278

Disclosure

The authors received materials support for this study from Novartis Pharma. The authors have received additional funding and materials support from Novartis Pharma for research separate to this submission. Prof. Little has received funding support from Amgen and Celgene and Dr Schindeler has received funding support from Celgene and N8 Medical for studies unrelated to this submission.

ABSTRACT

Sclerostin, encoded by the *Sost* gene, is an important negative regulator of bone formation that has been proposed to have a key role in regulating the response to mechanical loading. To investigate the effect of long-term Sclerostin deficiency on mechanotransduction in bone, we performed experiments on unloaded or loaded tibiae of 10 week old female *Sost*-/- and wild type mice. Unloading was induced via 0.5U BTX injections into the right quadriceps and calf muscles, causing muscle paralysis and limb disuse. On a separate group of mice, increased loading was performed on the left tibiae through unilateral cyclic axial compression of equivalent strains (+1200με) at 1200 cycles/day, 5days/week. Another cohort of mice receiving equivalent loads (-9.0N) also were assessed. Contralateral tibiae served as normal load controls. Loaded/unloaded and normal load tibiae were assessed at day 14 for bone volume (BV) and formation changes. Loss of BV was seen in the unloaded tibiae of wild type mice, but BV was not different between normal load and unloaded *Sost*-/- tibiae. An increase in BV was seen in the loaded tibiae of wild type and *Sost*-/- mice over their normal load controls. The increased BV was associated with significantly increased mid-shaft periosteal MS/BS, MAR and BFR/BS, and endosteal MAR and BFR/BS. Notably, loading induced a greater increase in periosteal MAR and BFR/BS in *Sost*-/- mice than in wild type controls. Thus, long-term Sclerostin deficiency inhibits the bone loss normally induced with decreased mechanical load, but can augment the increase in bone formation with increased load.

INTRODUCTION

Sclerostin, a secreted glycoprotein encoded by the *Sost* gene, is an important negative regulator of bone accumulation (1, 2). Sclerostin inhibits canonical Wnt signaling via blockade of low-density-lipoprotein receptor-related protein (LRP) receptors, including LRP5 and LRP6 (3). Sclerostin expression is specific to terminally differentiated cells embedded within mineralized matrix, including osteocytes, cementocytes and hypertrophic chondrocytes, but not osteoblasts or bone lining cells (1, 4-6). The major downstream effect of Sclerostin expression is the inhibition of osteoblastogenesis (6), although Sclerostin has also been shown to promote osteoclastogenesis (7, 8), via modulation of RANKL and OPG synthesis in osteocytes (9, 10).

The key role of Sclerostin in regulating bone homeostasis was identified via the human conditions van Buchem's disease and Sclerosteosis (11-14). Both result from mutations in the *Sost* gene, leading to increased bone formation and high bone mass. A comparable high bone mass and increased bone formation phenotype has been described in mouse models in which *Sost* is knocked-out (15, 16). This role of Sclerostin has led to inhibitory strategies for the prevention and treatment of bone loss in osteoporosis and metabolic bone disease. Animal and human trials of anti-Sclerostin antibodies have demonstrated increased bone formation and mass with treatment (17-22). Importantly, the effect on bone formation has been seen in models of osteoporosis and on resting bone surfaces along with remodeling surfaces.

Sclerostin has further been proposed to be a key regulator of mechanotransduction in bone. Increases in Sclerostin have been implicated in the bone loss associated with reduced loading. *Sost* mRNA expression was reported to increase in rodent models of limb disuse, and decline upon subsequent loading (23, 24). Mice deficient in Sclerostin, through genetic knock-out or short-term anti-Sclerostin antibody treatment, did not display the same extent of bone volume loss following hind limb unloading through tail suspension (25, 26). This result suggests that Sclerostin expression may mediate the response of bone to unloading. Discrepancies remain whether this bone loss inhibition is due to reduced bone anabolism, or rather decreased resorption. Conversely, *Sost* mRNA and Sclerostin protein expression were decreased following mechanical loading, and this reduction correlated with regions showing increased bone formation (23, 24). Importantly, in a transgenic mouse that constitutively expressed elevated Sclerostin levels, bone formation and bone volume gain associated with mechanical loading was inhibited (27). However, limited research has been undertaken to understand the

effect that Sclerostin deficiency has on bone's ability to respond to increased mechanical load. This investigation is important with the potential use of anti-Sclerostin antibodies.

The canonical Wnt/β-catenin pathway has many inhibitors and regulators, aside from Sclerostin. Other Wnt inhibitors, such as secreted Fzd-related-proteins (sFRPs) and Dickkopfs may have a role in Wnt inhibition within the bone compartment, or may be compensatory in the absence of Sclerostin. Interestingly, Dickkopf-1 (Dkk1) is up-regulated when Sclerostin is absent (28, 29). Further, Dkk1 might have a Wnt3a-independent effect on cyclooxygenase-2 (Cox-2) expression, an early mechanical loading induced transcript (30).

In this study we aimed to investigate the effects of long-term Sclerostin deficiency on mechanotransduction. Increased and decreased loading studies were performed on the *Sost*-/- mouse and age-matched wild type controls. Bone volume and formation changes in loaded/unloaded and contralateral tibiae were examined using a combination of micro-computed tomography (microCT) and histomorphometry outcome measures.

MATERIALS AND METHODS

Sost knockout mice

Sost-/- mice, previously described (14, 31), were backcrossed to C57BL/6J genetic background using founders with above 99.09% isogenicity/identity to the C57BL/6J strain. Age-matched *Sost*+/+ (wild type/WT) C57BL/6J control mice were obtained (Charles River Laboratories, Sulzfeld, Germany). All animal experiments were approved by the Western Sydney LHD Animal Ethics Committee, protocol 4174.

Botulinum toxin-induced tibial unloading

10 week old female *Sost*-/- and wild type mice (N=10/strain) were anesthetized (70mg/kg ketamine, 10mg/kg xylazine) and then injected with 0.5U botulinum toxin (BTX, Allergen) into both the right quadriceps and the right calf muscles. This treatment caused tibial unloading by muscle paralysis and limb disuse. After 24 hrs mice were unable to use their right hind limb. Left tibiae served as normal load controls. Mice were monitored throughout the study to ensure limb disuse was maintained; including assessing ability to grip, walk and stretch out the right hind limb. Weekly body weights were recorded (Supp. Fig. 1). Mice were injected with calcein (10mg/kg, Sigma Aldrich) 8 and 1 days before euthanasia, and euthanized at day 14. Post-harvest, hind limbs

(tibia, fibular, femur and muscle) were weighed excluding skin and feet, and fixed 24 hrs, 10% formalin and stored in 70% ethanol.

Tibial mid-diaphyseal strain gauging

As *Sost*-/- mice possessed denser bones than wild type, strain gauging was performed to calibrate the applied loading to reflect any stiffness differences present between the two genotypes. Strain (bone tissue deformation) levels at the midshaft of right and left tibiae were measured in 10 week old female *Sost*-/- and wild type mice (N=5/strain) as previously described (32). Briefly, mice were anesthetized (isoflurane inhalation) and a small incision made in the skin at the anterior tibia, half way down the bone. Muscle and periosteum were scraped away to expose the diaphysis, and the bone cleaned/dried with methyl ethyl ketone. A miniature single element strain gauge (EA-06-015LA-120, Vishay Micromeasurements) was attached to the medial midshaft aligned with the bone's longitudinal axis.

The left hind limb was placed into a custom made loading apparatus so that the heel and knee were cupped and held securely. A range of cyclic axial compressive loads, ranging -4 to -24N, were applied using a 4 Hz haversine waveform. No tibial failures occurred with the load range. The strain at each load increment was recorded (National Instruments, Labview v8.2). The relationship between the axial force applied and the strain on the tibial midshaft was determined for each genotype and was used to calculate the load required to achieve +1200με at the tibial mid-shaft for both the *Sost*-/- and wild type mice.

Cyclic tibial loading

10 week old female *Sost*-/- and wild type mice (N=10/strain) underwent unilateral cyclic axial compression of the left tibia. 1200 cycles were applied 5 days/week for 2 weeks, with rest on days 6, 7, 12 and 13. Equivalent loads for *Sost*-/- and wild type mice were applied to achieve +1200με on the mid-shaft. A separate cohort of wild type and *Sost*-/- mice all received -9.0N force to directly compare load-matched responses between the genotypes. Weekly body weights were recorded (Supp. Fig. 1).

Mice were injected with calcein (10mg/kg, Sigma) 10 and 3 days before euthanasia, and euthanized at day 14. Tibiae were fixed 24 hrs in 10% formalin and stored in 70% ethanol.

Dual-energy X-ray absorptiometry

Dual-energy X-ray absorptiometry (DXA) (GE Lunar PIXImus; Lunar Piximus Corp, Madison, WI) was performed at days 0, 7 and 14 for unloading and loading studies, either under isoflurane anesthesia or post-euthanasia. For unloading studies a region of interest of 20 pixels long by 13 pixels wide was positioned below the growth plate within the metaphysis, the region most responsive to unloading-induced bone loss. For loading studies a region of interest of 30 pixels long by 13 pixels wide was analyzed in the diaphysis, centered half-way along the tibia, to correlate with the region where the known strain was produced. Bone mineral density (BMD) and bone mineral content (BMC) were obtained.

MicroCT

Right and left tibiae from unloading/loading studies were microCT scanned (Skyscan 1174 2; Skyscan NV, Kontich, Belgium) using 12 μm isotropic voxel resolution, 0.5 mm aluminium filter, 50 kV X-ray tube voltage, 800 μA tube electric current, and 4500 ms exposure time. Images were reconstructed using a 0-0.1 greyscale (NRecon v1.6.1.7; Skyscan NV) and analysed with CTAnalyser (Skyscan NV). The minimum threshold for bone was 0.4 g/cm^3, determined through correlation to phantoms of known density.

All microCT analysis excluded the fibula. A volume of interest (VOI) denoted "7.8 mm VOI" was selected, commencing 0.5mm below the growth plate and finishing 7.8 mm distally, proximal to the tibia-fibula joint (Fig 1). Consecutive VOIs of height 0.06 mm were assessed along the 7.8 mm VOI to visualize bone volume change, between treated and control, along the loaded/unloaded tibiae. Sub-regional analysis was performed within the metaphysis and diaphysis (Fig 1). A metaphyseal VOI height of a 1.2 mm, commencing 0.5 mm below the growth plate, was denoted the metaphyseal "Canc+Cort" VOI as it assessed both the cancellous and cortical metaphyseal bone together. Within this region, a "Cancellous" only VOI was analysed by excluding the cortical sheath. The "Cortical" bone was also analyzed separately, excluding cancellous bone. Two diaphyseal VOIs of 0.5 mm height were assessed, 37% and 50% down the tibia from the proximal end. These VOIs correspond with other published studies that examine the response to increased load in the tibia (23, 32-34).

Bone parameters assessed within cancellous VOIs were trabecular bone volume (BV), trabecular bone volume/total volume (BV/TV), tissue volume (TV) and tissue mineral density (TMD), as well as microarchitecture parameters of trabecular thickness (Tb.Th), number (Tb.N) and separation (Tb.Sp). Within

cortical VOIs cortical BV, cortical thickness (Ct.Th) and TMD were assessed, as well as periosteal (Ps) and endosteal (Ec) surface and polar moment of inertia [MMI(polar)], a geometric predictor of whole bone strength. When the metaphyseal VOI contained cancellous and cortical bone then BV and TV were assessed.

Bone histomorphometry

Mineralized diaphyseal samples were embedded in methyl methacrylate and 5 μm transverse sections cut at two regions of interest in each tibia: 37% and 50% from the proximal end of the tibiae. Images were captured using a Leica DMLA CTRMC microscope (Leica Microsystems, Heerbrugg, Switzerland) and a QICAM Fast 1394 color 12 bit camera with QCapture software version 2.6.8.2 (Quantitative Imaging Corporation, British Columbia, Canada). The diaphyseal cortical bone was analyzed for daily mineral apposition rate (MAR), mineralizing surface/bone surface (MS/BS) and bone formation rate/bone surface (BFR/BS).

Coronal sections of the proximal tibiae were cut for metaphyseal cancellous bone assessment. Mineralized metaphyseal samples were cryosectioned (5 μm) using Cryofilm type IIC(10) (Section-Lab Co., Hiroshima, Japan) and images captured using Aperio Scanscope FL, Scanscope CS2 and Aperio Imagescope v11.2.0.780 (Aperio, Vista, CA, USA). Samples were analysed for MAR, MS/BS and BFR/BS. Sections were also stained for tartrate-resistant acid phosphatase (TRAP) and analysis performed for osteoclast number (N.Oc), osteoclast surface (Oc.S), and bone surface (BS), with the size of the osteoclast (Oc.S/BS) and the fraction of bone surface with osteoclasts adhered (Oc.S/BS) examined. All histomorphometry was performed with BIOQUANT measure 32 Nova Prime (Nashville, TN, USA).

Statistical analysis

Statistical analysis of strain gauge data between mouse genotypes was performed using non-parametric Mann-Whitney U test. Remaining statistical assessment between genotypes was performed using parametric independent sample t-test with a 95% confidence interval. Analysis of contralateral tibiae was performed using parametric paired samples test with a 95% confidence interval. Comparison of the effect of loading/unloading treatment between genotypes was analyzed via general linear analysis using univariate analysis of variance. For all testing a value of $p<0.05$ was considered significant. All analysis was performed using IBM SPSS Statistics 20 (SPSS Inc., Chicago, IL, USA).

RESULTS

Sclerostin deficiency prevents bone loss caused by unloading

Localized muscle wastage was evident following BTX treatment, with 26% decreases in weight of wild type and *Sost-/-* BTX-treated hind limbs versus their contralateral controls ($p<0.01$, Fig 2A). There were no differences in hind limb weight between genotypes when comparing treated hind-limbs only, or control hind limbs only.

Prior to BTX treatment the tibiae intended for unloading (right tibiae) of the wild type mice had significantly greater BMD within the metaphysis than contralateral control (left) tibiae, as measured by DXA (Fig 2B); likely due to manual positioning of ROIs for analysis. However, the response with unloading in wild type mice was such that metaphyseal BMD was significantly reduced (-8%) by day 14, compared to control tibiae ($p<0.01$). In contrast, longitudinal assessment by DXA in *Sost-/-* mice showed no significant change between the unloaded and control limbs in metaphyseal BMD at any time point. Percent change in BMD from day 0 was not related to body weight changes for the unloaded tibiae (Supp. Fig. 1). Metaphyseal BMC by DXA trended in response to unloading in a similar manner as BMD for wild type and *Sost-/-* mice (data not shown). MicroCT confirmed decreased bone volume with unloading in the wild type mice (-5%, $p<0.01$, Fig 2C), but there was no significant difference between the *Sost-/-* unloaded and contralateral tibiae. The BV change along the tibiae of wild type and *Sost-/-* mice was demonstrated in a histogram (Fig 2D).

Sub-regional microCT analyses were performed (Tables 1 and 2). In unloaded wild type tibiae, metaphyseal bone volume decreased 9% compared to the control limb ($p<0.01$). This decreased metaphyseal BV was within both cortical (-7%, $p<0.05$) and cancellous (-20%, $p<0.01$) bone. Cortical thickness (-10%, $p<0.01$) and cortical TMD (-3%, $p<0.05$) were also significantly decreased with unloading. This cortical bone loss in response to unloading appeared to be primarily on the endosteal surface with an increase in the endosteal perimeter (4%, $p<0.01$), and also an increase in TV of the cancellous region (9%, $p<0.01$). Cancellous BV/TV (-25%), Tb.N (-17%) and TMD (-8%) were all significantly decreased ($p<0.01$). The mid-diaphysis showed similarly a loss of bone in response to unloading. The two mid-diaphyseal VOIs showed significant decreases (between -5 and -8%) in BV and cortical thickness with unloading in the wild type tibiae ($p<0.01$). In the 37% cortical VOI the

endosteal perimeter was significantly increased (7%, $p<0.05$), suggesting localized widening of the marrow cavity at this region.

In the *Sost-/-* unloaded tibiae a statistically significant but small (-3%) decrease in cortical thickness was seen in the 50% cortical VOI ($p<0.05$). This decrease did not translate into changes on any other bone parameters, for either the 50% or 37% cortical VOIs.

Dynamic histomorphometry of control wild type and *Sost-/-* tibiae indicated that bone formation in the metaphysis of *Sost-/-* mice approached that of wild type mice by 12 weeks of (Fig 3). Further, unloading did not alter any of these bone formation parameters in wild type or *Sost-/-* mice, suggesting bone formation was not the major responder to decreased loading. However, no changes were seen in N.Oc, Oc.S/N.Oc, or Oc.S/BS with unloading compared to control tibiae for wild type and *Sost-/-* mice, suggesting no unloading-related changes in osteoclast size or the fraction of bone surface with osteoclasts adhered. Wild type control and unloaded tibiae did have significantly greater Oc.S/BS compared to *Sost-/-* control and unloaded tibiae ($p<0.01$). This difference is likely due to a greater bone surface in the *Sost-/-* mice as N.Oc was not changed between the mouse strains or treatment.

Variation of bone strain in Sclerostin deficient mice

The *Sost-/-* tibiae showed a trend towards increased stiffness under the same compressive cyclic loading force compared to wild type control mice. While this difference did not reach significance ($p=0.09$, Fig 4), a *post-hoc* power analysis indicated based on the effect size (Cohen d value = 1.24) that the observed power (β) was 0.32. Based on the high effect size both strain matched and force matched experiments were carried out. For strain-matched experiments, the *Sost-/-* and wild type mice received -12.5 N and -9.0 N force respectively to induce equivalent strains of 1200 με on the mid-diaphysis of the tibiae. For force matched experiments, separate groups of *Sost-/-* and wild type mice received -9.0 N loading.

Sclerostin deficiency results in increased load-induced bone formation

Prior to loading (day 0) the relative BMD of wild type tibial mid-diaphyses intended for loading (left tibiae) was less than that of the contralateral controls (right tibiae) ($p<0.05$) as measured by DXA (Fig 5A); likely due to manual positioning of ROIs for analysis. However, the response of strain-matched loading by day 14 was a

significant increase in diaphyseal BMD over controls (16%, $p<0.01$). No difference in BMD was seen at day 0 between the loaded/contralateral *Sost*-/- tibiae by DXA (Fig 5A). Notably, diaphyseal BMD was significantly increased in the strain-matched *Sost*-/- mice following loading (11% at day 7, 23% at day 14; $p<0.01$). Change in BMD over the study period was not related to body weight changes (Supp. Fig. 1). Diaphyseal BMC trended similarly to BMD in wild type and *Sost*-/- mice by DXA (data not shown).

Loading-induced increases in BV was confirmed by MicroCT in wild type and *Sost*-/- mice at day 14 ($p<0.01$, Fig 5B). The 20% BV increase in strain-matched *Sost*-/- tibiae was significantly greater than the 15% BV increase in wild type tibiae ($p<0.01$). These BV increases were constant along the 7.8mm diaphyseal region that was analyzed (Fig 5C). Similar BMD and bone volume responses to loading were also seen in the load-matched study for the *Sost*-/- mice (Fig 6). This confirmed that the response to loading in the *Sost*-/- mice was not only a result of the increased load applied in the strain-matched study.

As strain engendered on the bone, rather than an external load, correlates with mechanotransduction responses (35-38), further microCT sub-regional analysis was performed for the strain-matched loading cohort of mice. Within the metaphysis effects with loading were similar in the wild type and *Sost*-/- mice (Table 1). BV was increased in the loaded tibiae compared to their contralateral controls, but only within the cortical bone compartment ($p<0.01$). The 29% increase in *Sost*-/- cortical BV was significantly greater than the 13% increase in WT tibiae ($p<0.01$). The cortical thickness of this metaphyseal sheath was increased for both wild type and *Sost*-/- loaded tibiae, due to increases in their periosteal perimeters ($p<0.01$). A small 2% TMD increase was seen in the *Sost*-/- loaded metaphyseal cortex only ($p<0.01$). No change in BV or BV/TV was seen in the cancellous metaphyseal bone of the wild type mice, while *Sost*-/- mice had a significant decrease in cancellous BV and BV/TV with loading (-13% and -7%, $p<0.05$). However, TV of the cancellous compartment was also 5% decreased in the *Sost*-/- loaded mice ($p<0.01$), suggesting a shift towards cortical bone within the metaphyseal VOI of the *Sost*-/- tibiae.

The cortical bone within the two mid-diaphyseal VOIs (37%, 50% along the tibiae respectively) showed similar results to the metaphyseal cortical bone (Table 2). There were significant increases seen in BV (17%, 19% wild type; 19%, 13% *Sost*-/-), Ct.Th (16%, 17% wild type; 16%, 10% *Sost*-/-), and periosteal perimeter (5%, 8% wild type; 5%, 4% *Sost*-/-) ($p<0.01$), suggesting periosteal expansion. These resulted in increased MMI(polar)

in both wild type (26%, 30%) and *Sost*-/- (30%, 20%) loaded tibiae compared to their contralateral controls ($p<0.01$). A small 2% increase in TMD was seen within the 37% VOI for *Sost*-/- loaded tibiae only ($p<0.01$).

Dynamic histomorphometry of non-loaded control tibiae of the wild type and *Sost*-/- mice indicated that bone formation in the mid-diaphysis of *Sost*-/- mice approached that of wild type mice by 12 weeks of age (Fig 7). Within the metaphyseal cancellous bone MS/BS, MAR and BFR/BS were not different between the genotypes. Within the mid-diaphysis (37% cortical ROI) MS/BS was significantly increased in the *Sost*-/- control tibiae compared to wild type control ($p<0.01$), but MAR and BFR/BS were not different between the genotypes on either the periosteal or endosteal surfaces. Comparable findings were noted at the mid-diaphyseal 50% cortical ROI (data not shown).

Periosteal and endosteal responses were both seen with loading of wild type and *Sost*-/- mice. On the periosteal surface, MS/BS, MAR and BFR/BS were all significantly increased compared to the contralateral control tibiae ($p<0.01$). The MAR and BFR/BS response was greater in *Sost*-/- mice than wild type ($p<0.01$). Endosteal MAR ($p<0.01$) and BFR ($p<0.05$) were also significantly increased for wild type and *Sost*-/- mice. However, MS/BS was decreased on this surface for both wild type ($p<0.01$) and *Sost*-/- loaded tibiae ($p<0.05$).

DISCUSSION

This study comprehensively investigates the response of the *Sost*-/- mouse line to increased cyclic loading and Botox-induced unloading. Sclerostin plays a major role in mechanotransduction in bone. Acute and chronic Sclerostin deficiency can prevent bone loss associated with reduced loading (25, 26) and upregulation of Sclerostin can prevent increases in bone volume associated with increased loading (27). We hypothesized that the response of bone to mechanical loading and unloading would be significantly impaired in the absence of Sclerostin, in comparison to C57Bl/6J wild type controls.

Contrary to our initial hypothesis, *Sost*-/- mice responded positively to a cyclic load protocol; cortical bone volume increased significantly in both *Sost*-/- and control mice, and correlated with increased bone formation. While Sclerostin has been identified as a key factor in the anabolic response of bone to load, our results indicate an alternative Sclerostin-independent mechanism. While prior findings indicate that Sclerostin down-regulation within osteocytes is necessary for bone response to loading (27), our data suggest that *Sost* deficiency is not sufficient to induce maximal bone anabolism, and that anabolism can be further increased with mechanical

load. Further, an enhanced bone formation response to increased load was seen in the *Sost*-/- tibiae. MAR and BFR/BS responses on the periosteal mid-diaphyseal surfaces of the *Sost-/-* tibiae were increased compared to the wild type responses. These data indicate an increased response to strain-matched loading with *Sost* deficiency.

While the anabolic response to load is not dependent on Sclerostin, unloading-induced bone loss was attenuated in *Sost-/-* mice. This is consistent with the prior literature showing Sclerostin to be a key modulator of unloading induced bone loss (25, 26, 39). Direct resorption assessment would provide clearer information of this effect on catabolism, as the osteoclast parameters measured only reflect their resorption activity. However, as bone formation was not effected by unloading this appears to disregard bone anabolism changes as the primary response of decrease bone volume with unloading.

These results of loading and unloading regimes in a situation of long-term Sclerostin deficiency provide clinically relevant findings. Human studies of bed-rest have reported elevated Sclerostin levels, suggesting that anti-Sclerostin treatment may target the mechanism of bone loss (40, 41). These data support the clinical utility of anti-Sclerostin therapies for treating boss loss associated with unloading, such as disuse osteopenia. Further, the benefit of encouraging exercise/bone loading for individuals with osteoporosis receiving anti-Sclerostin therapy is unknown. These data raise the possibility that exercise may provide an additive anabolic effect on bone even in the presence of Sclerostin blockade. However, this hypothesis will need to be validated via controlled clinical studies.

The Sclerostin-independent bone response to increased load indicates the involvement of other factors in bone mechanotransduction. Other inhibitors of the canonical Wnt/β-catenin signaling pathway may have a role in mechanotransduction, acting along-side Sclerostin or taking up such a role where Sclerostin is deficient. Such compensation may be the cause of the comparable metaphyseal and diaphyseal bone formation parameters between *Sost-/-* and wild type control tibiae at 12 weeks age. A key candidate is Dkk1 which is up-regulated in the Sclerostin knock-out mouse and within van Buchem and Sclerosteosis patients (28, 29). Elevated Dkk1 levels within the bone compartment could down-regulate in response to increased load, leading to increased Wnt/β-catenin signaling and bone formation. Further, a more intricate system independent of, or in synergy with, the Wnt/β-catenin pathway may be involved in bone modulation. Factors of interest include estrogen

receptor α (ERα), insulin-like growth factor 1 (IGF-1), parathyroid hormone (PTH), leptin, prostanoids, PGE2, connexin 43, interleukin-11 and bone morphogenetic proteins (BMPs) (30, 42-47).

Future work investigating other potential mechanotransduction modulators is required. Such prospective modulators may be highlighted by gene and protein expression analysis following loading/unloading and also studies of longer loading/unloading periods. In particular, prolonged unloading in a Sclerostin deficient system has not been studied in detail and compensatory responses may emerge with longer unloading. Moreover, investigation of models that feature deficiency in multiple Wnt pathway regulators may reveal compensation or synergy with Sclerostin, or suggest modulators outside the Wnt pathway.

Bone volume was increased in diaphyseal and metaphyseal cortical bone of wild type and *Sost-/-* mice. The metaphyseal bone response was greater in the *Sost-/-* tibiae than the wild type tibiae, and could reflect site-specific differences in mechanical strain induced on the two genotypes. The strains induced when loading the *Sost-/-* and wild type bones were measured and calibrated, but only the diaphyseal strains could be concluded as equivalent. Differences in bone volume, stiffness and geometry between the genotypes may affect the strain engendered within the metaphysis. However, bone compartment specific responses to changes in Wnt/β-catenin signaling are known and may support the site-specific responses seen in the *Sost-/-* tibiae as true effects (28, 39).

An anabolic bone response to loading was not seen within metaphyseal cancelleous bone of either *Sost-/-* or wild type mice. Further, the overall tissue volume of the metaphyseal cancellous region was reduced in the *Sost-/-* mice. These data suggest a generalized corticalisation of the *Sost-/-* metaphysis in response to increased loading.

The lack of an anabolic cancelleous response is in contrast to other similar loading regimes within the literature (32-34, 48), likely due to the age of the mice used, the mechanical strain engendered or the VOIs selected. An age-dependent response of cancellous bone to loading has been shown, particularly when comparing growing mice versus adult mice (48). Further, studies with a cancellous bone response in C57Bl/6 mice, of comparable age and loading regimes as our investigation, were either loaded to induce a higher tibial mid-shaft strain, or were measured with more rudimentary VOIs (32-34). These VOIs were cylinder volumes positioned within the marrow space of the metaphysis, providing only a representative examination of the cancellous bone. Our study provided a more expansive investigation. This does highlight the challenge of comparing results of published

loading/unloading studies, with no commonly accepted standards for analysis. Other variables such as sex, loading period/regime and mouse strain may also be responsible for inconsistencies in wild type responses within the literature. Of particular note, with emerging evidence of ERα involvement in mechanotransduction there may be gender specific effects confounding comparisons (30, 44).

Some limitations existing within this study are worth note. Littermate controls, unavailable to us, would have provided optimal controls. Back-crossing of founder *Sost-/-* mice, of 99.09% isogenicity/identity to the C57BL/6J strain, supports minimum strain differences; however genetic drift between the two colonies cannot be completely discounted. Further, age-matched non-treated mice would provide rigorous baseline controls, confirming contralateral tibiae as suitable controls. There is the potential for compensation by control limbs following treatment of the contralateral limbs, particularly in the BTX model. Previous murine unloading studies utilising BTX to induce hind-limb disuse have shown moderate systemic effects resulting in a lowering of bone mass in the contralateral (non-treated) tibiae compared to baseline controls, likely a result of reduced activity (49, 50). However, this does not discount the comparative effect of unloaded tibia.

Despite these limitations, this study presents direct comparison of increased and decreased load responses in Sclerostin deficient bone, and provides novel information about the role of Sclerostin in mechanotransduction. Although Sclerostin loss-of-function offers protection from unloading induced bone loss, it does not prevent bone gain in response to increased load but rather results in an increased bone formation response. Thus while Sclerostin may be involved in bone mechanotransduction, it is not the sole modulator of the loading response. Future work is required to elucidate other factors that are essential for sensing and transducing mechanotransduction signals in response to bone load.

ACKNOWLEDGMENTS

This project received funding from the Elizabeth Rosenthal Bone Research Bequest and Departmental funds. Travel funding was awarded through the Burroughs Wellcome Travel grant and the University of Sydney Postgraduate Research Scholarship Scheme. Novartis Pharma provided materials support (mice). The project received funding support for equipment costs from National Institutes of Health grant R01-AG028664. Dr Schindeler received salary support from NHMRC Project Grant 1003478.

Authors' roles: Study design: DGL, MCHM, MMM, MK and AM. Study conduct: AM, NHK and KMM. Data collection: AM. Data interpretation: AM, MMM, DGL, MCHM, MK and IK. Drafting manuscript: AM. Revising manuscript content: AS, MCHM, MMM, DGL and IK. Approving final version of manuscript: all authors. AM takes responsibility for the integrity of the data analysis.

REFERENCES

1. Poole KE, van Bezooijen RL, Loveridge N, Hamersma H, Papapoulos SE, Lowik CW, et al. Sclerostin is a delayed secreted product of osteocytes that inhibits bone formation. FASEB journal : official publication of the Federation of American Societies for Experimental Biology. 2005;19(13):1842-4.

2. van Bezooijen RL, ten Dijke P, Papapoulos SE, Lowik CW. SOST/sclerostin, an osteocyte-derived negative regulator of bone formation. Cytokine & growth factor reviews. 2005;16(3):319-27.

3. Semenov M, Tamai K, He X. SOST is a ligand for LRP5/LRP6 and a Wnt signaling inhibitor. J Biol Chem. 2005;280(29):26770-5.

4. van Bezooijen RL, Bronckers AL, Gortzak RA, Hogendoorn PC, van der Wee-Pals L, Balemans W, et al. Sclerostin in mineralized matrices and van Buchem disease. Journal of dental research. 2009;88(6):569-74.

5. Jager A, Gotz W, Lossdorfer S, Rath-Deschner B. Localization of SOST/sclerostin in cementocytes in vivo and in mineralizing periodontal ligament cells in vitro. Journal of periodontal research. 2010;45(2):246-54.

6. van Bezooijen RL, Roelen BA, Visser A, van der Wee-Pals L, de Wilt E, Karperien M, et al. Sclerostin is an osteocyte-expressed negative regulator of bone formation, but not a classical BMP antagonist. The Journal of experimental medicine. 2004;199(6):805-14.

7. Glass DA, 2nd, Bialek P, Ahn JD, Starbuck M, Patel MS, Clevers H, et al. Canonical Wnt signaling in differentiated osteoblasts controls osteoclast differentiation. Dev Cell. 2005;8(5):751-64.

8. Spencer GJ, Utting JC, Etheridge SL, Arnett TR, Genever PG. Wnt signalling in osteoblasts regulates expression of the receptor activator of NFkappaB ligand and inhibits osteoclastogenesis in vitro. Journal of cell science. 2006;119(Pt 7):1283-96.

9. Wijenayaka AR, Kogawa M, Lim HP, Bonewald LF, Findlay DM, Atkins GJ. Sclerostin stimulates osteocyte support of osteoclast activity by a RANKL-dependent pathway. PLoS One. 2011;6(10):e25900.

10. Kramer I, Halleux C, Keller H, Pegurri M, Gooi JH, Weber PB, et al. Osteocyte Wnt/beta-catenin signaling is required for normal bone homeostasis. Molecular and cellular biology. 2010;30(12):3071-85.

11. Staehling-Hampton K, Proll S, Paeper BW, Zhao L, Charmley P, Brown A, et al. A 52-kb deletion in the SOST-MEOX1 intergenic region on 17q12-q21 is associated with van Buchem disease in the Dutch population. American journal of medical genetics. 2002;110(2):144-52.

12. Balemans W, Ebeling M, Patel N, Van Hul E, Olson P, Dioszegi M, et al. Increased bone density in sclerosteosis is due to the deficiency of a novel secreted protein (SOST). Human molecular genetics. 2001;10(5):537-43.

13. Gardner JC, van Bezooijen RL, Mervis B, Hamdy NA, Lowik CW, Hamersma H, et al. Bone mineral density in sclerosteosis; affected individuals and gene carriers. J Clin Endocrinol Metab. 2005;90(12):6392-5.

14. Loots GG, Kneissel M, Keller H, Baptist M, Chang J, Collette NM, et al. Genomic deletion of a long-range bone enhancer misregulates sclerostin in Van Buchem disease. Genome Res. 2005;15(7):928-35.

15. Kramer I, Kneissel M. The high bone mass phenotype of Sost deficient mice is characterized by progressive increase in bone thickness, mineralization and predicted cortical bone strength in a gene dosage unrelated manner. Bone. 2008;42, Supplement 1(0):S57.

16. Li X, Ominsky MS, Niu QT, Sun N, Daugherty B, D'Agostin D, et al. Targeted deletion of the sclerostin gene in mice results in increased bone formation and bone strength. J Bone Miner Res. 2008;23(6):860-9.

17. Li X, Warmington KS, Niu QT, Asuncion FJ, Barrero M, Grisanti M, et al. Inhibition of sclerostin by monoclonal antibody increases bone formation, bone mass, and bone strength in aged male rats. J Bone Miner Res. 2010;25(12):2371-80.

18. Li X, Ominsky MS, Warmington KS, Morony S, Gong J, Cao J, et al. Sclerostin antibody treatment increases bone formation, bone mass, and bone strength in a rat model of postmenopausal osteoporosis. J Bone Miner Res. 2009;24(4):578-88.

19. Li X, Warmington KS, Niu QT, Asuncion FJ, Barrero M, Grisanti M, et al. Inhibition of sclerostin by monoclonal antibody increases bone formation, bone mass, and bone strength in aged male rats. J Bone Miner Res. 2010;25(12):2647-56.

20. Ominsky MS, Vlasseros F, Jolette J, Smith SY, Stouch B, Doellgast G, et al. Two doses of sclerostin antibody in cynomolgus monkeys increases bone formation, bone mineral density, and bone strength. J Bone Miner Res. 2010;25(5):948-59.

21. Padhi D, Jang G, Stouch B, Fang L, Posvar E. Single-dose, placebo-controlled, randomized study of AMG 785, a sclerostin monoclonal antibody. J Bone Miner Res. 2011;26(1):19-26.

22. McClung MR, Grauer A, Boonen S, Bolognese MA, Brown JP, Diez-Perez A, et al. Romosozumab in Postmenopausal Women with Low Bone Mineral Density. The New England journal of medicine. 2014.

23. Moustafa A, Sugiyama T, Prasad J, Zaman G, Gross T, Lanyon L, et al. Mechanical loading-related changes in osteocyte sclerostin expression in mice are more closely associated with the subsequent osteogenic response than the peak strains engendered. Osteoporosis International. 2011:1-10.

24. Robling AG, Niziolek PJ, Baldridge LA, Condon KW, Allen MR, Alam I, et al. Mechanical stimulation of bone in vivo reduces osteocyte expression of Sost/sclerostin. J Biol Chem. 2008;283(9):5866-75.

25. Lin C, Jiang X, Dai Z, Guo X, Weng T, Wang J, et al. Sclerostin mediates bone response to mechanical unloading through antagonizing Wnt/beta-catenin signaling. J Bone Miner Res. 2009;24(10):1651-61.

26. Spatz JM, Ellman R, Cloutier AM, Louis L, van Vliet M, Suva LJ, et al. Sclerostin antibody inhibits skeletal deterioration due to reduced mechanical loading. J Bone Miner Res. 2013;28(4):865-74.

27. Tu X, Rhee Y, Condon KW, Bivi N, Allen MR, Dwyer D, et al. Sost downregulation and local Wnt signaling are required for the osteogenic response to mechanical loading. Bone. 2012;50(1):209-17.

28. Chang MK, Kramer I, Keller H, Gooi JH, Collett C, Jenkins D, et al. Reversing LRP5-dependent osteoporosis and SOST-deficiency induced sclerosing bone disorders by altering WNT signaling activity. J Bone Miner Res. 2013.

29. van Lierop A, Moester M, Hamdy N, Papapoulos S. Serum Dickkopf 1 Levels in Sclerostin Deficiency. J Clin Endocrinol Metab. 2013.

30. Liedert A, Wagner L, Seefried L, Ebert R, Jakob F, Ignatius A. Estrogen receptor and Wnt signaling interact to regulate early gene expression in response to mechanical strain in osteoblastic cells. Biochem Biophys Res Commun. 2010;394(3):755-9.

31. Kramer I, Loots GG, Studer A, Keller H, Kneissel M. Parathyroid hormone (PTH)-induced bone gain is blunted in SOST overexpressing and deficient mice. J Bone Miner Res. 2010;25(2):178-89.

32. Lynch ME, Main RP, Xu Q, Walsh DJ, Schaffler MB, Wright TM, et al. Cancellous bone adaptation to tibial compression is not sex dependent in growing mice. J Appl Physiol. 2010;109(3):685-91.

33. Fritton JC, Myers ER, Wright TM, van der Meulen MC. Bone mass is preserved and cancellous architecture altered due to cyclic loading of the mouse tibia after orchidectomy. J Bone Miner Res. 2008;23(5):663-71.

34. Fritton JC, Myers ER, Wright TM, van der Meulen MC. Loading induces site-specific increases in mineral content assessed by microcomputed tomography of the mouse tibia. Bone. 2005;36(6):1030-8.

35. Gross TS, Edwards JL, McLeod KJ, Rubin CT. Strain gradients correlate with sites of periosteal bone formation. J Bone Miner Res. 1997;12(6):982-8.

36. Mosley JR, Lanyon LE. Strain rate as a controlling influence on adaptive modeling in response to dynamic loading of the ulna in growing male rats. Bone. 1998;23(4):313-8.

37. Torrance AG, Mosley JR, Suswillo RF, Lanyon LE. Noninvasive loading of the rat ulna in vivo induces a strain-related modeling response uncomplicated by trauma or periostal pressure. Calcif Tissue Int. 1994;54(3):241-7.

38. Mosley JR, March BM, Lynch J, Lanyon LE. Strain magnitude related changes in whole bone architecture in growing rats. Bone. 1997;20(3):191-8.

39. Macias BR, Aspenberg P, Agholme F. Paradoxical Sost gene expression response to mechanical unloading in metaphyseal bone. Bone. 2013;53(2):515-9.

40. Gaudio A, Pennisi P, Bratengeier C, Torrisi V, Lindner B, Mangiafico RA, et al. Increased sclerostin serum levels associated with bone formation and resorption markers in patients with immobilization-induced bone loss. J Clin Endocrinol Metab. 2010;95(5):2248-53.

41. Spatz JM, Fields EE, Yu EW, Divieti Pajevic P, Bouxsein ML, Sibonga JD, et al. Serum sclerostin increases in healthy adult men during bed rest. J Clin Endocrinol Metab. 2012;97(9):E1736-40.

42. Price JS, Sugiyama T, Galea GL, Meakin LB, Sunters A, Lanyon LE. Role of Endocrine and Paracrine Factors in the Adaptation of Bone to Mechanical Loading. Curr Osteoporos Rep. 2011.

43. Bonewald LF, Johnson ML. Osteocytes, mechanosensing and Wnt signaling. Bone. 2008;42(4):606-15.

44. Zaman G, Saxon LK, Sunters A, Hilton H, Underhill P, Williams D, et al. Loading-related regulation of gene expression in bone in the contexts of estrogen deficiency, lack of estrogen receptor alpha and disuse. Bone. 2010;46(3):628-42.

45. Sunters A, Armstrong VJ, Zaman G, Kypta RM, Kawano Y, Lanyon LE, et al. Mechano-transduction in osteoblastic cells involves strain-regulated estrogen receptor alpha-mediated control of insulin-like growth factor (IGF) I receptor sensitivity to Ambient IGF, leading to phosphatidylinositol 3-kinase/AKT-dependent Wnt/LRP5 receptor-independent activation of beta-catenin signaling. J Biol Chem. 2010;285(12):8743-58.

46. Gross TS, Srinivasan S, Liu CC, Clemens TL, Bain SD. Noninvasive loading of the murine tibia: an in vivo model for the study of mechanotransduction. J Bone Miner Res. 2002;17(3):493-501.

47. Kesavan C, Wergedal JE, Lau KH, Mohan S. Conditional disruption of IGF-I gene in type 1alpha collagen-expressing cells shows an essential role of IGF-I in skeletal anabolic response to loading. American journal of physiology Endocrinology and metabolism. 2011;301(6):E1191-7.

48. De Souza RL, Matsuura M, Eckstein F, Rawlinson SC, Lanyon LE, Pitsillides AA. Non-invasive axial loading of mouse tibiae increases cortical bone formation and modifies

trabecular organization: a new model to study cortical and cancellous compartments in a single loaded element. Bone. 2005;37(6):810-8.

49. Warner SE, Sanford DA, Becker BA, Bain SD, Srinivasan S, Gross TS. Botox induced muscle paralysis rapidly degrades bone. Bone. 2006;38(2):257-64.

50. Marchand-Libouban H, Le Drevo MA, Chappard D. Disuse induced by Botulinum toxin affects the bone marrow expression profile of bone genes leading to a rapid bone loss. J Musculoskelet Neuronal Interact. 2013;13(1):27-36.

Figure Legends

Figure 1. A 7.8mm VOI of the tibia starting 0.5 mm below the proximal growth plate was assessed. Sub-regional analysis was performed in 3 VOIs. **VOI 1 (Metaphyseal Canc+Cort)** represents metaphyseal bone with 1.2mm height starting 0.5mm below the growth plate. The **Cortical** and **Cancellous** bone compartments of this VOI were analysed separately and together. **VOI 2 (37% Cortical)** and **VOI 3 (50% Cortical)** represents diaphyseal cortical bone in two 0.5 mm height VOIs situated 37% and 50% down from the proximal tibia.

Figure 2. Control and unloaded tibiae of WT (wild type) and *Sost-/-* mice: **(A)** End point weight of control and BTX-treated hind limbs: tibia, fibula, femur and muscle, excluding skin and feet; **(B)** DXA measured mean bone mineral (BMD) of the tibial metaphysis at days 0, 7, and 14. Bars represent ± SD; **(C)** MicroCT measured mean bone volume, within the 7.8 mm VOI of the tibiae. Bars represent + SD; **(D)** Bone volume change between unloaded and control tibiae along the 7.8 mm VOI. 1-3. Localities of sub-regional VOIs: 1. Metaphyseal VOI, 2. 37% Cortical VOI, 3. 50% Cortical VOI. ** $p<0.01$

Figure 3. Histomorphometric analysis of unloaded and control wild type (WT) and *Sost-/-* tibiae within metaphyseal cancellous bone. MS/BS, mineralizing surface/bone surface; MAR, mineral apposition rate/day; BFR/BS, bone formation rate/bone surface; N.Oc, osteoclast number; Oc.S/N.Oc, osteoclast surface/osteoclast number; Oc.S/BS, osteoclast surface/bone surface. Bars represent + SD, n=8-10 per group. ** $p<0.01$, * $p<0.05$.

Figure 4. Mean stiffness of wild type (WT) and *Sost-/-* tibiae measured by strain gauging of the mid-diaphysis. *Sost-/-* tibiae trended towards being stiffer than WT controls ($p=0.09$). Bars represent ± SD, n=4-5 per group.

Figure 5. Control and strain-matched (1200με) loaded tibiae of WT (wild type) and *Sost-/-* mice: **(A)** DXA measured mean bone mineral (BMD) of the tibial diaphysis at days 0, 7, and

14. Bars represent ± SD; **(B)** MicroCT measured mean bone volume, within the 7.8 mm VOI of the tibiae. Bars represent + SD; **(C)** Bone volume change between loaded and control tibiae along the 7.8 mm VOI. 1-3. Localities of sub-regional VOIs: 1. Metaphyseal VOI, 2. 37% Cortical VOI, 3. 50% Cortical VOI. ** $p<0.01$

Figure 6. Control and load-matched (-9.0N) loaded tibiae of WT (wild type) and *Sost*-/- mice: **(A)** DXA measured mean bone mineral (BMD) of the tibial diaphysis at days 0, 7, and 14. Bars represent ± SD; **(B)** MicroCT measured mean bone volume, within the 7.8 mm VOI of the tibiae. Bars represent + SD; **(C)** Bone volume change between loaded and control tibiae along the 7.8 mm VOI. 1-3. Localities of sub-regional VOIs: 1. Metaphyseal VOI, 2. 37% Cortical VOI, 3. 50% Cortical VOI. ** $p<0.01$, * $p<0.05$

Figure 7. Histomorphometric analysis of strain-matched (1200με) loaded and control wild type (WT) and *Sost*-/- tibiae within the diaphyseal 37% Cortical VOI. **(A)** Periosteal and endosteal surfaces were analysed for: MS/BS, mineralizing surface/bone surface; MAR mineral apposition rate/day; BFR/BS, bone formation rate/bone surface. Bars represent + SD, n=8-10 per group. ** $p<0.01$, * $p<0.05$. **(B)** Representative images of Calcein bone labeling.

Table 1. Metaphyseal bone parameters measured by MicroCT for strain-matched (1200με) loading and unloading studies. a = $p<0.01$, b = $p<0.05$ compared to contralateral control.

		Loading Study				Unloading Study			
		WT		*Sost-/-*		WT		*Sost-/-*	
Metaphyseal VOI	Parameters	Control	Loaded	Control	Loaded	Control	Unloaded	Control	Unloaded
Canc+Cort	TV (mm^3)	3.03 ± 0.15	3.31 ± 0.18[a]	3.30 ± 0.20	3.78 ± 0.25[a]	3.05 ± 0.14	3.09 ± 0.16	3.34 ± 0.19	3.44 ± 0.24[b]
	BV (mm^3)	1.74 ± 0.12	1.94 ± 0.11[a]	2.35 ± 0.17	2.85 ± 0.21[a]	1.63 ± 0.10	1.49 ± 0.08[a]	2.32 ± 0.18	2.34 ± 0.19
Cancellous	TV (mm^3)	1.36 ± 0.08	1.42 ± 0.13	1.28 ± 0.09	1.21 ± 0.10[a]	1.49 ± 0.06	1.62 ± 0.10[a]	1.44 ± 0.09	1.51 ± 0.12
	BV (mm^3)	0.23 ± 0.04	0.23 ± 0.07	0.48 ± 0.09	0.42 ± 0.10[b]	0.25 ± 0.05	0.20 ± 0.03[a]	0.56 ± 0.06	0.60 ± 0.11
	BV/TV (%)	16.91 ± 2.96	16.25 ± 4.16	37.10 ± 4.93	34.54 ± 6.15[b]	16.50 ± 3.33	12.45 ± 1.44[a]	38.53 ± 3.26	39.48 ± 5.77
	Tb.Th (mm)	0.09 ± 0.00	0.10 ± 0.00[a]	0.14 ± 0.04	0.13 ± 0.01	0.08 ± 0.00	0.08 ± 0.00[a]	0.12 ± 0.00	0.12 ± 0.01
	Tb.Sp (mm)	0.27 ± 0.03	0.28 ± 0.03	0.22 ± 0.06	0.22 ± 0.03	0.25 ± 0.02	0.25 ± 0.01	0.17 ± 0.01	0.17 ± 0.02
	Tb.N (mm^{-1})	1.90 ± 0.28	1.61 ± 0.35[b]	2.81 ± 0.56	2.63 ± 0.38	1.98 ± 0.32	1.65 ± 0.17[a]	3.17 ± 0.20	3.32 ± 0.42
	TMD (g/cm^3)	0.64 ± 0.03	0.68 ± 0.03[a]	0.80 ± 0.04	0.82 ± 0.04	0.64 ± 0.03	0.59 ± 0.02[a]	0.89 ± 0.18	0.83 ± 0.05
Cortical	BV (mm^3)	1.51 ± 0.09	1.70 ± 0.08[a]	1.87 ± 0.12	2.42 ± 0.20[a]	1.38 ± 0.08	1.29 ± 0.09[b]	1.75 ± 0.16	1.75 ± 0.16
	Ct.Th (mm)	0.24 ± 0.01	0.26 ± 0.01[a]	0.30 ± 0.1	0.37 ± 0.02[a]	0.21 ± 0.01	0.19 ± 0.01[a]	0.26 ± 0.02	0.26 ± 0.02
	Ps (mm)	7.10 ± 0.28	7.33 ± 0.22[a]	7.22 ± 0.25	7.56 ± 0.29[a]	7.31 ± 0.26	7.22 ± 0.24	7.47 ± 0.24	7.46 ± 0.16
	Ec (mm)	5.61 ± 0.24	5.73 ± 0.29	5.45 ± 0.32	5.41 ± 0.40	5.97 ± 0.22	6.18 ± 0.20[a]	5.94 ± 0.28	6.20 ± 0.32
	TMD (g/cm^3)	1.31 ± 0.04	1.35 ± 0.05	1.46 ± 0.02	1.49 ± 0.03[a]	1.27 ± 0.04	1.23 ± 0.04[b]	1.43 ± 0.04	1.43 ± 0.06
n		10	10	10	10	10	10	10	10

Table 2. Diaphyseal bone parameters measured by MicroCT for strain-matched (1200με) loading and unloading studies. a = $p<0.01$, b = $p<0.05$ compared to contralateral control.

		Loading Study				Unloading Study			
		WT		*Sost-/-*		WT		*Sost-/-*	
Diaphyseal VOI	Parameters	Control	Loaded	Control	Loaded	Control	Unloaded	Control	Unloaded
37% Cortical	BV (mm^3)	0.55 ± 0.03	0.64 ± 0.03[a]	0.74 ± 0.05	0.88 ± 0.05[a]	0.50 ± 0.02	0.47 ± 0.02[a]	0.68 ± 0.06	0.68 ± 0.06
	Ct.Th (mm)	0.26 ± 0.01	0.30 ± 0.01[a]	0.34 ± 0.00	0.39 ± 0.01[a]	0.24 ± 0.01	0.22 ± 0.00[a]	0.31 ± 0.01	0.31 ± 0.02
	Ps (mm)	5.84 ± 0.26	6.14 ± 0.25[a]	6.06 ± 0.29	6.34 ± 0.29[a]	5.75 ± 0.19	5.68 ± 0.27	5.94 ± 0.33	5.95 ± 0.26
	Ec (mm)	3.66 ± 0.14	3.74 ± 0.22	3.51 ± 0.26	3.69 ± 0.45	3.85 ± 0.23	4.11 ± 0.27[b]	3.95 ± 0.42	3.96 ± 0.30
	MMI(polar) (mm^4)	0.48 ± 0.06	0.60 ± 0.07[a]	0.67 ± 0.10	0.87 ± 0.11[a]	0.42 ± 0.03	0.41 ± 0.06	0.61 ± 0.10	0.62 ± 0.09
	TMD (g/cm^3)	1.47 ± 0.03	1.48 ± 0.04	1.56 ± 0.03	1.59 ± 0.02[a]	1.39 ± 0.04	1.39 ± 0.07	1.52 ± 0.03	1.52 ± 0.04
50% Cortical	BV (mm^3)	0.41 ± 0.02	0.49 ± 0.03[a]	0.60 ± 0.04	0.68 ± 0.05[a]	0.38 ± 0.01	0.36 ± 0.02[a]	0.56 ± 0.03	0.55 ± 0.03
	Ct.Th (mm)	0.28 ± 0.00	0.32 ± 0.02[a]	0.37 ± 0.00	0.41 ± 0.01[a]	0.26 ± 0.00	0.24 ± 0.00[a]	0.36 ± 0.01	0.35 ± 0.01[b]
	Ps (mm)	4.10 ± 0.16	4.42 ± 0.17[a]	4.66 ± 0.25	4.85 ± 0.22[b]	4.13 ± 0.14	4.05 ± 0.17	4.48 ± 0.23	4.51 ± 0.24
	Ec (mm)	2.23 ± 0.12	2.31 ± 0.23	2.31 ± 0.36	2.29 ± 0.45	2.48 ± 0.19	2.50 ± 0.15	2.45 ± 0.33	2.35 ± 0.20
	MMI(polar) (mm^4)	0.19 ± 0.03	0.25 ± 0.03[a]	0.31 ± 0.05	0.37 ± 0.06[a]	0.17 ± 0.02	0.17 ± 0.02	0.28 ± 0.04	0.28 ± 0.03
	TMD (g/cm^3)	1.65 ± 0.03	1.64 ± 0.05	1.73 ± 0.04	1.74 ± 0.02	1.52 ± 0.05	1.53 ± 0.06	1.66 ± 0.04	1.67 ± 0.04
n		10	10	10	10	10	10	10	10

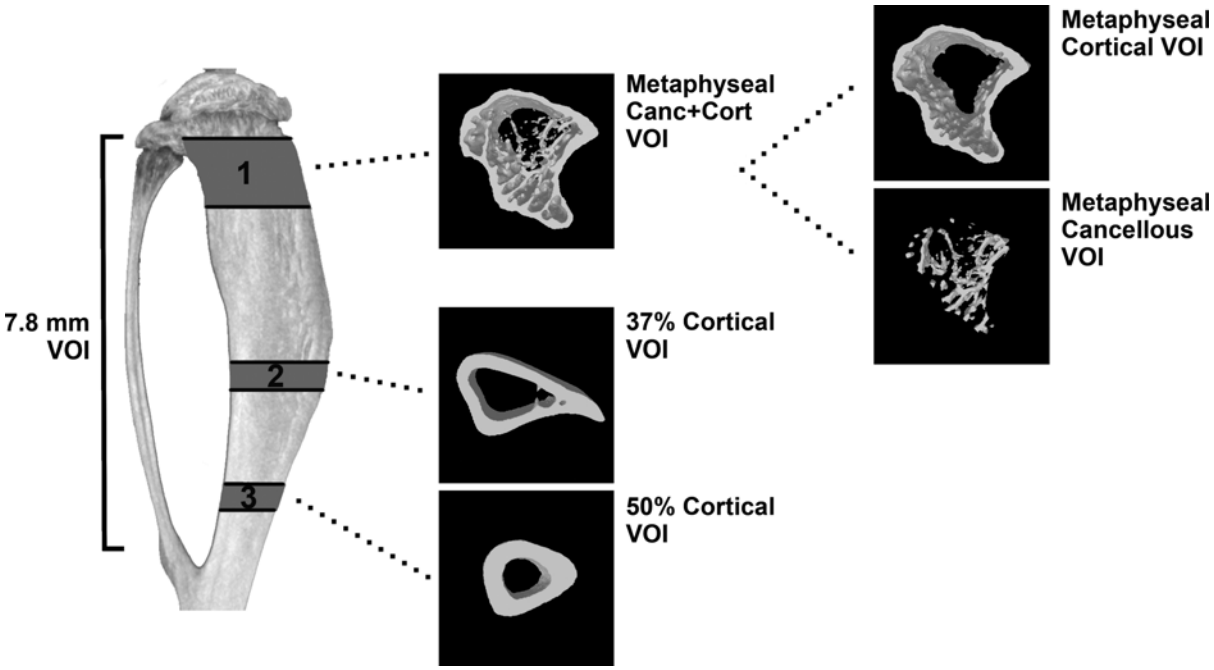

Figure 1

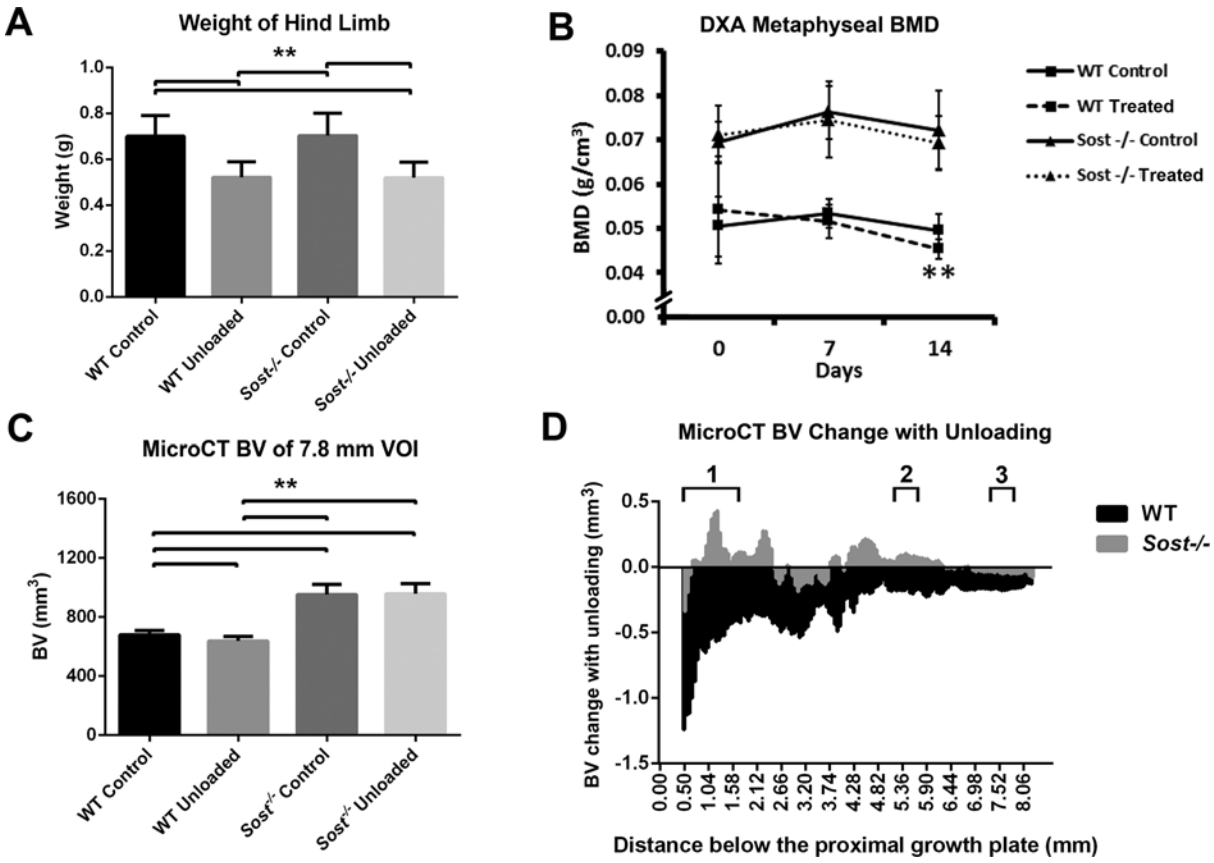

Figure 2

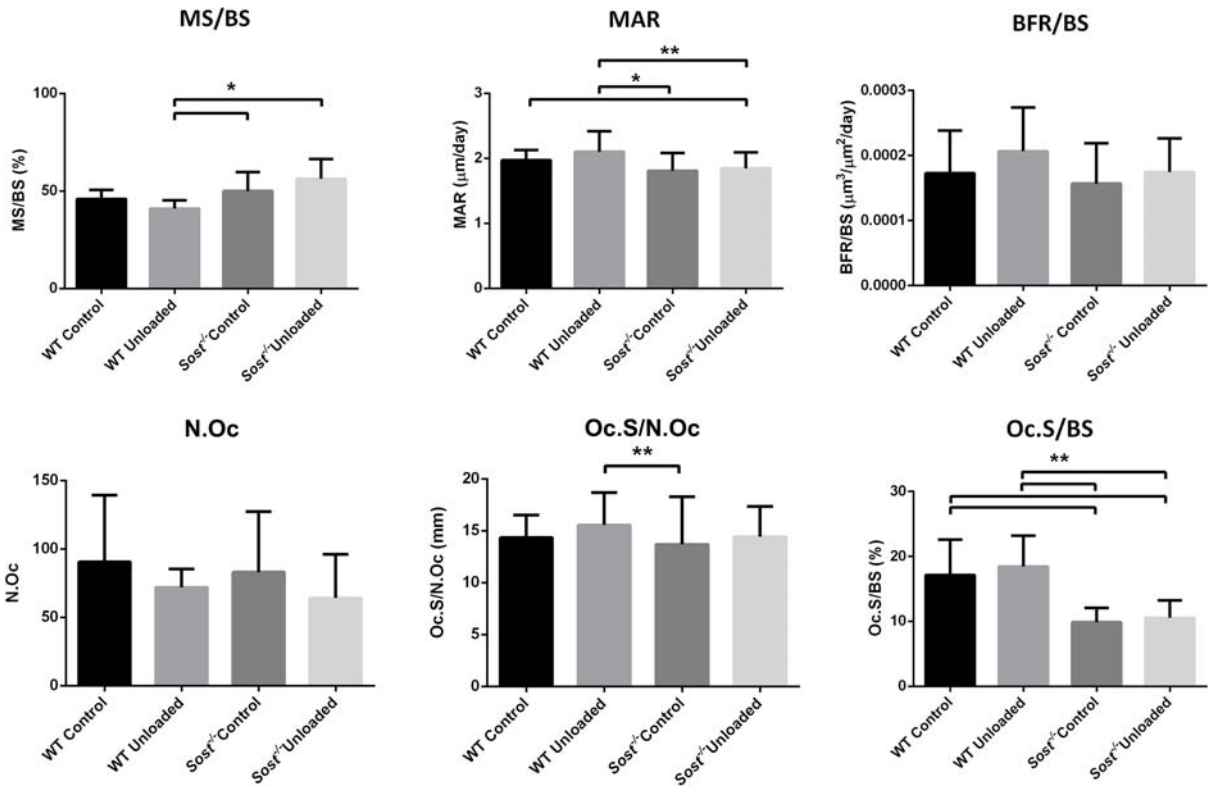

Figure 3

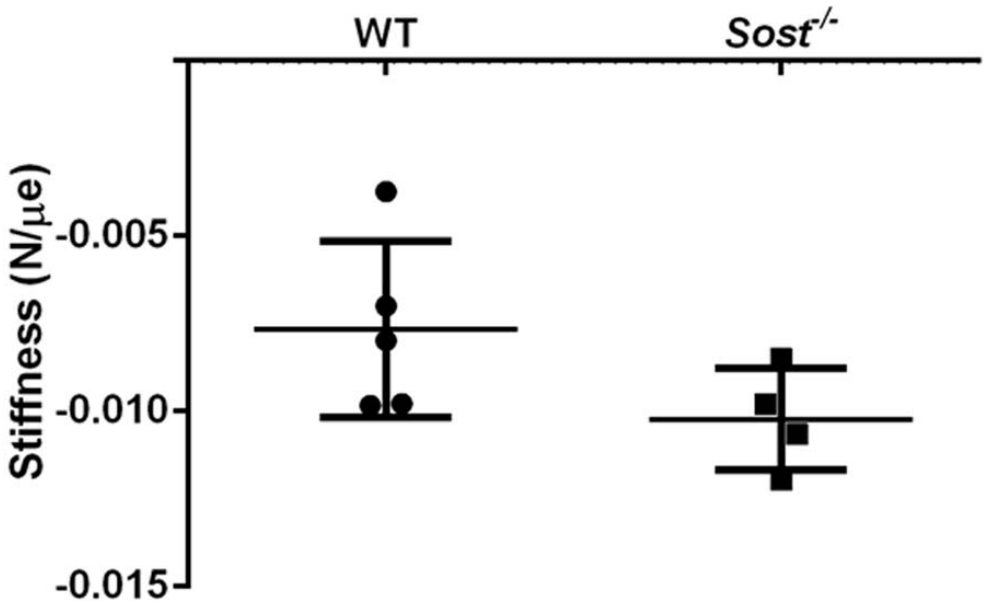

Figure 4

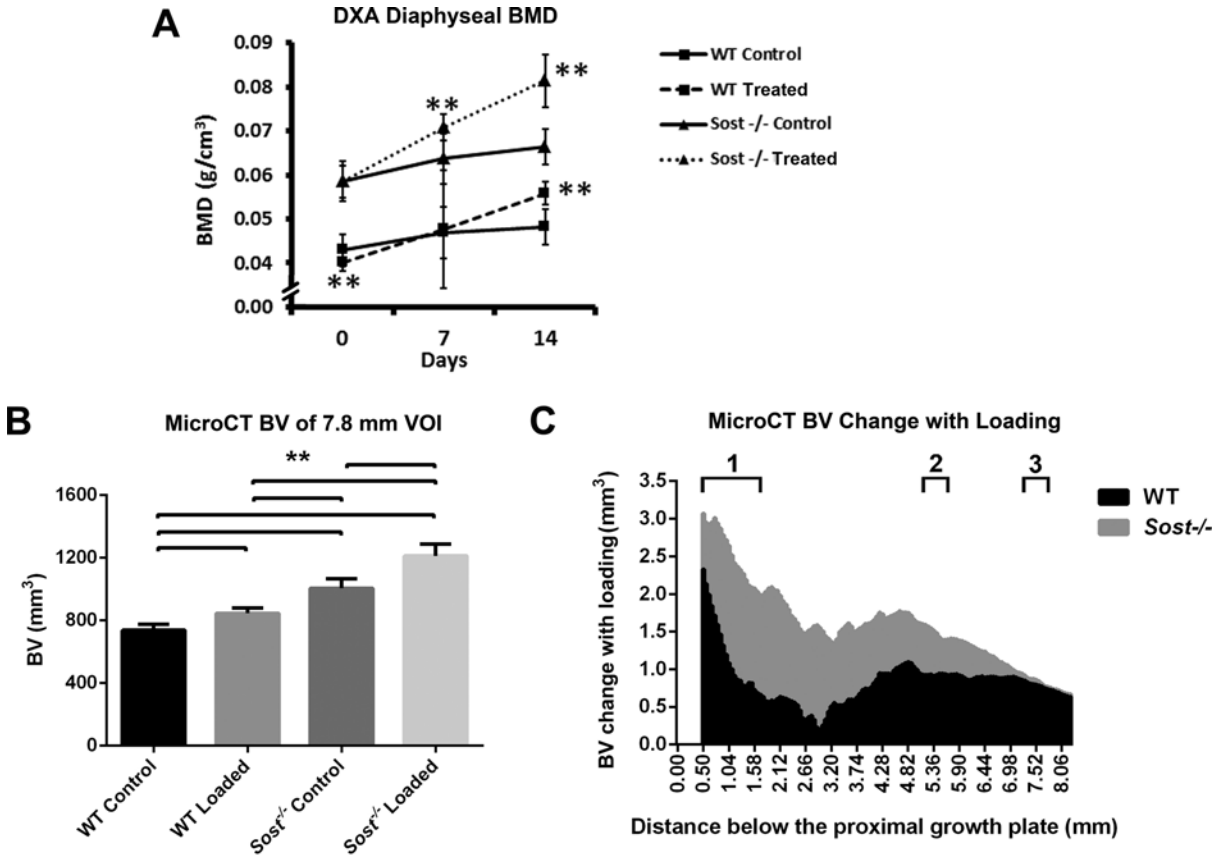

Figure 5

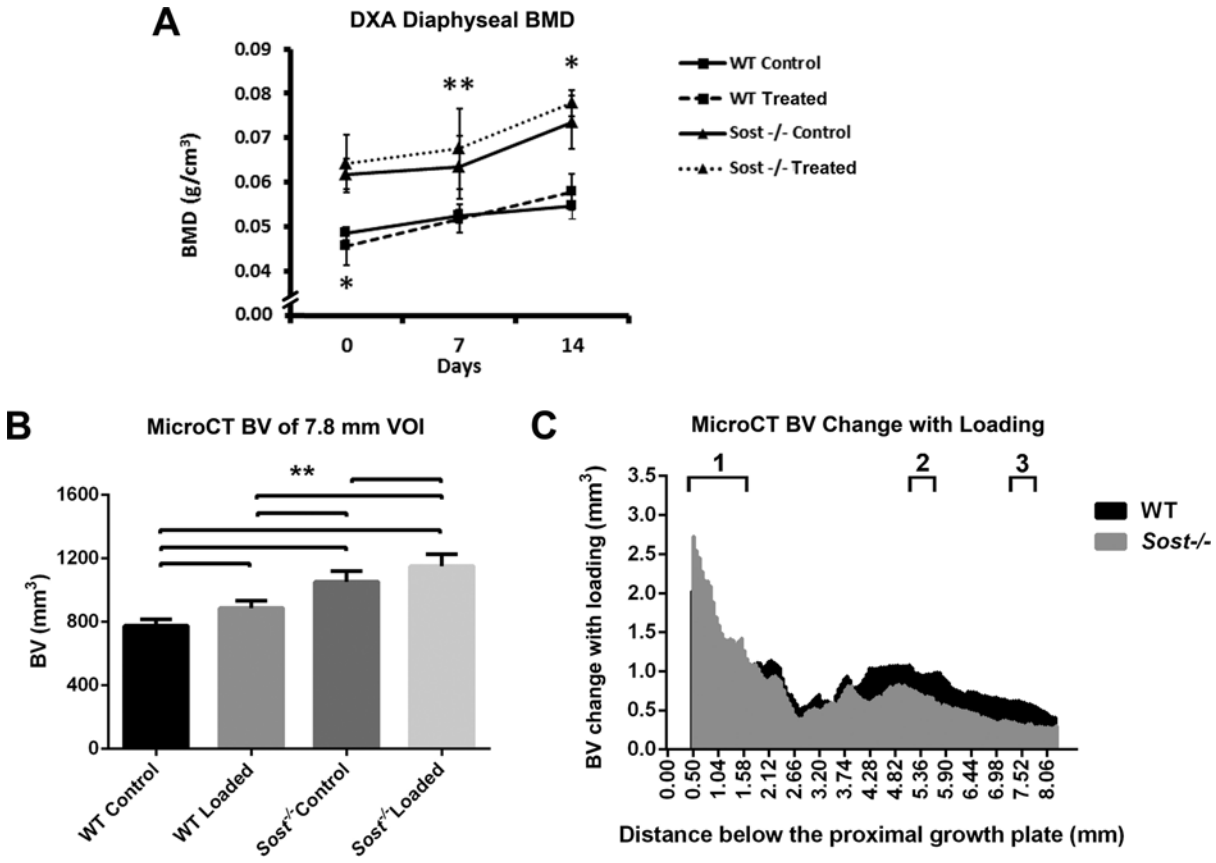

Figure 6

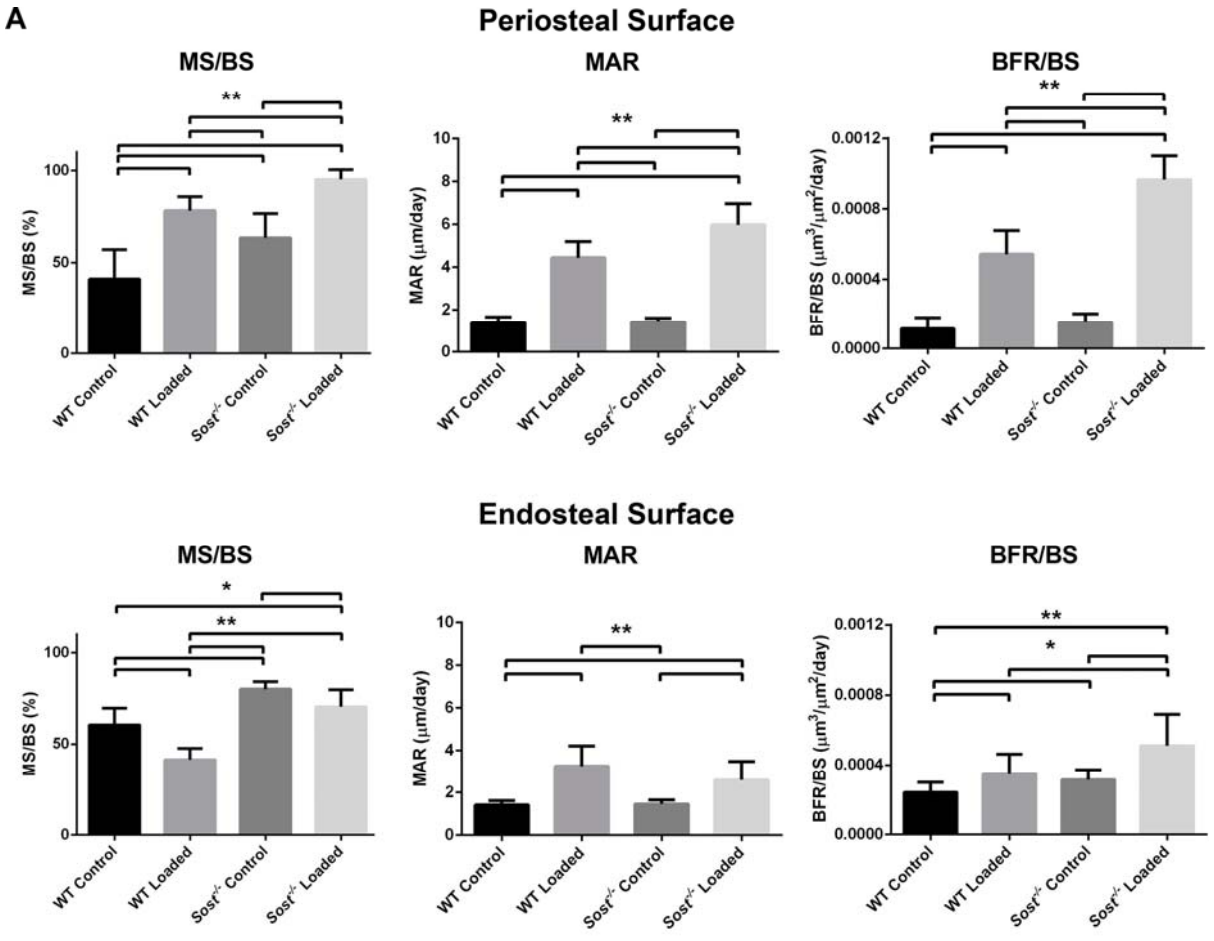

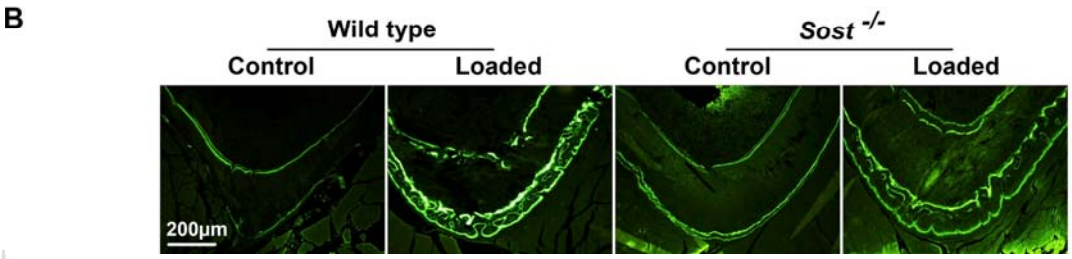

Figure 7